JACS
JOURNAL OF THE AMERICAN CHEMICAL SOCIETY
pubs.acs.org/JACS
Article

Collective Quantum Magnetism in Nitrogen-Doped Nanographenes

Gucheng Zhu,[#] Yashi Jiang,[#] Ying Wang,[#] Bing-Xin Wang, Yuqiang Zheng, Yufeng Liu, Li-Xia Kang, Zhanbo Li, Dandan Guan, Yaoyi Li, Hao Zheng, Canhua Liu, Jinfeng Jia, Tao Lin, Pei-Nian Liu,* Deng-Yuan Li,* and Shiyong Wang*

Cite This: J. Am. Chem. Soc. 2023, 145, 7136−7146

Read Online

ACCESS | Metrics & More | Article Recommendations | Supporting Information

ABSTRACT: The emergence of quantum magnetism in nanographenes provides ample opportunities to fabricate purely organic devices for spintronics and quantum information. Although heteroatom doping is a viable way to engineer the electronic properties of nanographenes, the synthesis of doped nanographenes with collective quantum magnetism remains elusive. Here, a set of nitrogen-doped nanographenes (N-NGs) with atomic precision are fabricated on Au(111) through a combination of imidazole [2+2+2]-cyclotrimerization and cyclodehydrogenation reactions. High-resolution scanning probe microscopy measurements reveal the presence of collective quantum magnetism for nanographenes with three radicals, with spectroscopic features which cannot be captured by mean-field density functional theory calculations but can be well reproduced by Heisenberg spin model calculations. In addition, the mechanism of magnetic exchange interaction of N-NGs has been revealed and compared with their counterparts with pure hydrocarbons. Our findings demonstrate the bottom-up synthesis of atomically precise N-NGs which can be utilized to fabricate low-dimensional extended graphene nanostructures for realizing ordered quantum phases.

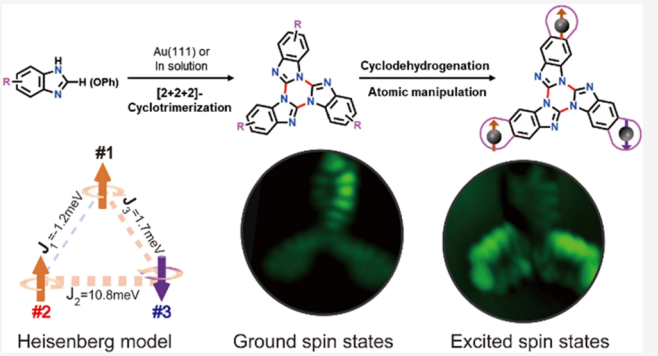

INTRODUCTION

Graphene nanomaterial, with negligible spin−orbit coupling, is an ideal platform to realize quantum nanomagnets with spin-rotation symmetry and collective quantum excitations.[1,2] The unpaired spins in nanographenes interact with each other via exchange interaction, forming collective quantum states which can be captured by Heisenberg model calculations. The magnetism of nanographenes originates from the emergence of unpaired electrons in their π-bond topology, which can be qualitatively captured by drawing non-kekulé structures.[3] Sublattice imbalance, topological frustration, and topological defects of π-bond topology can introduce unpaired π-electrons, giving highly tunable magnetic ground states.[2,4−8] Although theoretical studies got started in the 1950s, experimental realization of magnetic nanographenes has been achieved only recently.[9−16] The experimental lag is mainly because the magnetic nanographenes are usually unstable under ambient conditions, and the synthesis of unsubstituted large nanographene molecules using traditional synthetic chemistry is a great challenge due to the poor solubility and high reactivity.[17] In the past decade, a bottom-up approach has been developed as a modern method to synthesize nanographenes with precise controllability and wide tunability, in which chemical reactions are triggered at atomically flat metal substrates starting with properly designed molecular precursors under ultra-high-vacuum conditions.[18,19] Many magnetic nanographenes have been fabricated on surfaces, and their low-lying spin states have been detected by scanning tunneling spectroscopy (STS), with examples as triangulenes,[9,20−25] Clar goblets,[5] and metal-free porphyrins.[26−28] Collective excitations of quantum magnetism have been observed in triangulene dimers,[23] triangulene rings[21] and chains,[29] and metal-free porphyrin chains.[27] Recently, the interplay of quantum spins in nanographenes and cooper pairs in superconductors has been observed.[30] These results suggest that nanographenes host intrinsic quantum magnetism with great potential for applications in spintronics and quantum information.

Heteroatom substitution of graphene nanostructures provides an effective way to engineer their electronic and magnetic properties. For example, the incorporation of N dopants at the edges of graphene nanoribbons (GNRs) locally tunes the electron filling and results in atomically sharp GNR heterostructures.[31−33] Nitrogen or boron atom doping inside the GNR center, not at edges, introduces localized magnetic

Received: October 9, 2022
Published: March 23, 2023

https://doi.org/10.1021/jacs.2c10711
J. Am. Chem. Soc. 2023, 145, 7136−7146

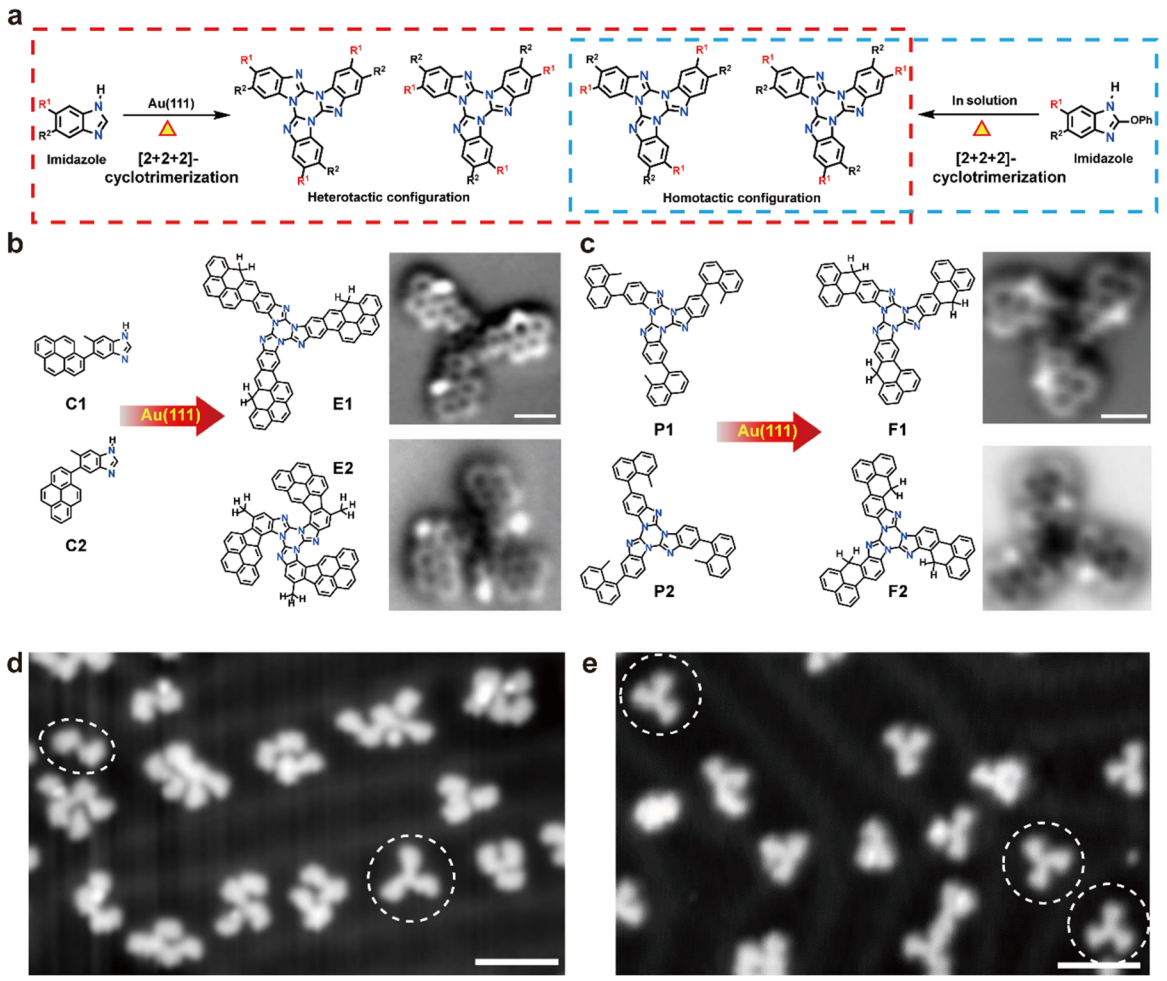

Figure 1. On-surface synthesis of N-NGs via imidazole [2+2+2]-cyclotrimerization and cyclodehydrogenation. (a) Imidazole [2+2+2]-cyclotrimerization pathways on Au(111) and in solution. (b) Chemical structures of imidazole precursors (C1 and C2) with two different adsorption configurations and nc-AFM images (resonant frequency: 26 kHz, oscillation amplitude: 80 pm, scale bars: 0.5 nm) of the corresponding [2+2+2]-cyclotrimerization products (E1 and E2). (c) Chemical structures of in-solution synthesized imidazole trimerization precursors (P1 and P2) and nc-AFM images (resonant frequency: 26 kHz, oscillation amplitude: 80 pm, scale bars: 0.5 nm) of the corresponding cyclodehydrogenation products (F1 and F2). (d, e) Overview STM images (bias: 100 mV, current: 10 pA, scale bars: 3 nm) of synthesized N-NGs on the Au(111) surface from (d) imidazoles (C1 and C2) and (e) in-solution pre-prepared imidazole trimerization precursors (P1 and P2), respectively.

moments near the dopants by breaking the sublattice balance of GNR π-bond topology.[34−38] Recently, nitrogen atom substitution has been used to modify the electronic properties of nanographenes, observing dication and tunable magnetic ground states.[25,39−41] However, the synthesis of heteroatom-doped nanographenes with collective quantum magnetism remains scarce.

The chemical reactivity of aromatic compounds can be substantially modified by introducing heteroatoms. For example, pyridine, pyrimidine, or imidazole groups are more reactive than their carbon counterparts, which have been widely used to realize efficient and selective coupling reactions in solution. During the past decade, intense efforts have been devoted to exploring controllable on-surface covalent reactions using heteroatom-substituted groups. Substantial progresses have been made in this direction with examples of controllable regiospecific C−H activation,[42] [1+1+1] cycloaddition,[43] [3+2] cycloaddition,[44] azide-alkyne cycloaddition,[45] carboxyl−amine coupling,[46] and cyclopentamerization,[47] to name a few. The introduction of rich and excellent chemical reactivity by heteroatom substitution provides a flexible toolbox for the fabrication of complex graphene nanostructures which may be retractable by using molecular precursors with pure carbons. Complex covalent single molecules, one-dimensional chains, and even two-dimensional networks with nitrogen substitutions have been fabricated on surfaces.[25,36,40,41,46−56] Bearing efficient and selective coupling reactions and the ability to tune electronic properties, heteroatom doping provides a promising route to realize ordered quantum phases in extended nanographene networks, which remains a formidable challenge in the field of carbon quantum magnetism.

Here, we fabricate a set of nitrogen-doped nanographenes (N-NGs) on Au(111) using on-surface or in-solution [2+2+2]-cyclotrimerization reactions of imidazole, followed by on-surface cyclodehydrogenation. Scanning tunneling microscopy (STM) and non-contact atomic force microscopy (nc-AFM) are used to characterize different products at the single-chemical-bond level. On-surface [2+2+2]-cyclotrimerization of imidazole gives a set of N-NGs with both homotactic and heterotactic configurations. To realize coupling selectivity, imidazole [2+2+2]-cyclotrimerization is first conducted in-solution, and then on-surface cyclodehydrogenation is

https://doi.org/10.1021/jacs.2c10711
J. Am. Chem. Soc. 2023, 145, 7136−7146

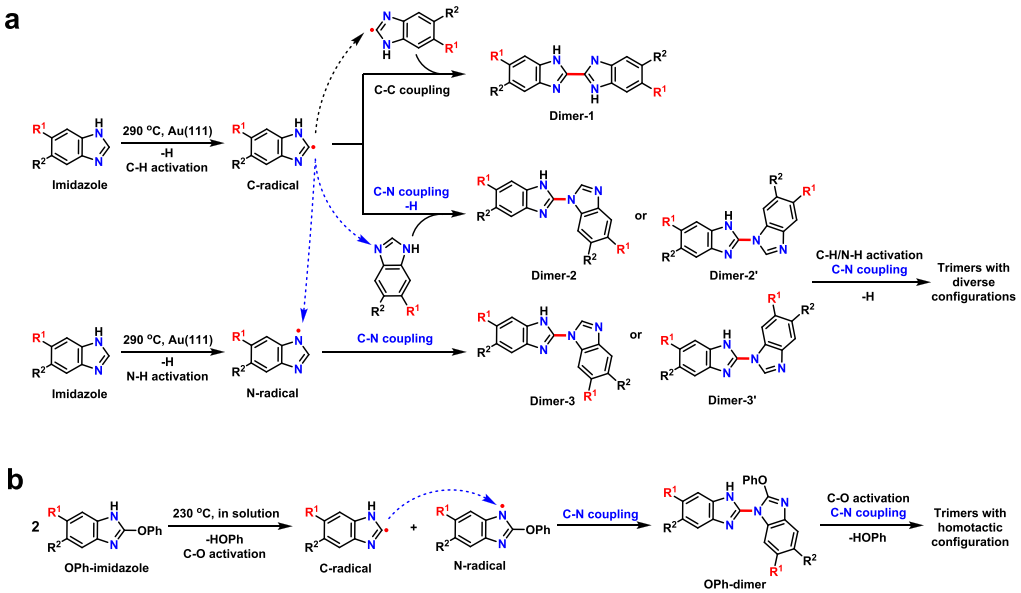

Figure 2. Polymerization pathways of imidazole (a) on the Au(111) surface and (b) in solution.

triggered on Au(111), which gives rise to purely homotactic N-NGs. We attribute the selective imidazole trimerization in-solution not on-surface to different ways of initiating reactions and coupling pathways. Scanning tunneling spectroscopy (STS) measurements reveal the presence of spin-singlet, doublet, triplet, and quartet states in different N-NGs, which can be explained by combined density functional theory (DFT) and Heisenberg spin model calculations. The mechanism of exchange interaction has been revealed and compared with their pure hydrocarbon counterparts. Our results demonstrate that heteroatom doping is not only an effective way to engineer the magnetic ground states of nanographenes but also provides a versatile toolbox to fabricate complex functional nanographenes, sought-after as new-generation organic materials in spintronics, photoluminescence, and quantum information.

RESULTS AND DISCUSSION

On-Surface Synthesis of N-NGs via Imidazole [2+2+2]-Cyclotrimerization and Cyclodehydrogenation. Imidazole, as an important aromatic five-membered heterocycle, has two *meta*-substituted nitrogen atoms, which makes it unique chemoselectivity in synthetic reactions. Therefore, polymerization of imidazole or its derivatives in solution or solid-state has been used to construct the diverse imidazole dimers and trimers.[57,58] However, direct polymerization of imidazole on surfaces has not been explored, which may be a promising approach for the synthesis of atomically precise N-NGs. As shown in Figure 1a, this part illustrates the [2+2+2]-cyclotrimerization of imidazole on two different dimensions, namely, a two-dimensional Au(111) surface and a three-dimensional solution. Due to the two-dimensional surface confinement, there are four kinds of trimers with two homotactic configurations and two heterotactic configurations on Au(111) (marked by a red dashed square). Instead, the imidazole [2+2+2]-cyclotrimerization in solution is highly selective and gives rise to only two trimerization products with pure homotactic configurations (indicated by a blue dashed square). This difference may be attributed to the following two facts: (1) the ways of initiating reactions to form the highly active carbon radical intermediates, in which the Au(111) surface is through C−H activation and the solution is through C−O activation;[58] (2) the driving force of maintaining reactions, in which Au(111) is the release of hydrogen atoms and the solution is the release of phenols (Figure 2).

Initially, 6-methyl-5-(pyren-1-yl)-1*H*-benzo[*d*]imidazole was used as a model molecular precursor, which may host two different adsorption configurations (C1 and C2) due to the Au(111) surface confinement (Figure 1b). Imidazole polymerization and cyclodehydrogenation on Au(111) occur after deposition and thermal annealing to 290 °C for 10 min, affording a set of clover-like and bilobed structures (indicated by a white dashed circle and ellipse in Figure 1d, respectively) in the STM image, which can be assigned to the imidazole trimer and dimer, respectively. High-resolution nc-AFM images (Figure 1b) show two representative bond-resolved [2+2+2]-cyclotrimerization products with heterotactic and homotactic configurations, consistent with the reaction scheme in Figure 1a. A frequently observed bilobal structure was also identified by STM and nc-AFM imaging (Figure S5b), showing two kinds of imidazole dimers that are from the on-surface dehydrogenation homo- and cross-coupling of two imidazoles C2, respectively. Notably, a four-lobed structure was also occasionally observed in the STM images (Figure S5b), which may be attributed to the imidazole tetramer, suggesting an on-surface [2+2+2+2]-cyclotetramerization pathway of imidazole. The statistical analysis by counting the number of imidazole reactants in large-scale STM images (Figure S6) reveals that the total ratio of coupling reactants is greater than 95% (Figure S7), in which the total ratio of C−N coupling (66%) is approximately twice that of the C−C coupling (31%). In the formed coupling products, the most abundant is the dimer involving C−C and C−N coupling, followed by the trimer involving C−N coupling. The tetramer and other oligomers are less abundant than the trimer.

To clarify the reaction pathways of imidazole polymerization on Au(111), we conduct DFT calculations for the imidazole polymerization process including C−H and N−H activation (Figure S8) and subsequent C−C (Figure S9) and C−N coupling (Figure S10) by using 1*H*-benzo[*d*]imidazole as a

https://doi.org/10.1021/jacs.2c10711
J. Am. Chem. Soc. 2023, 145, 7136−7146

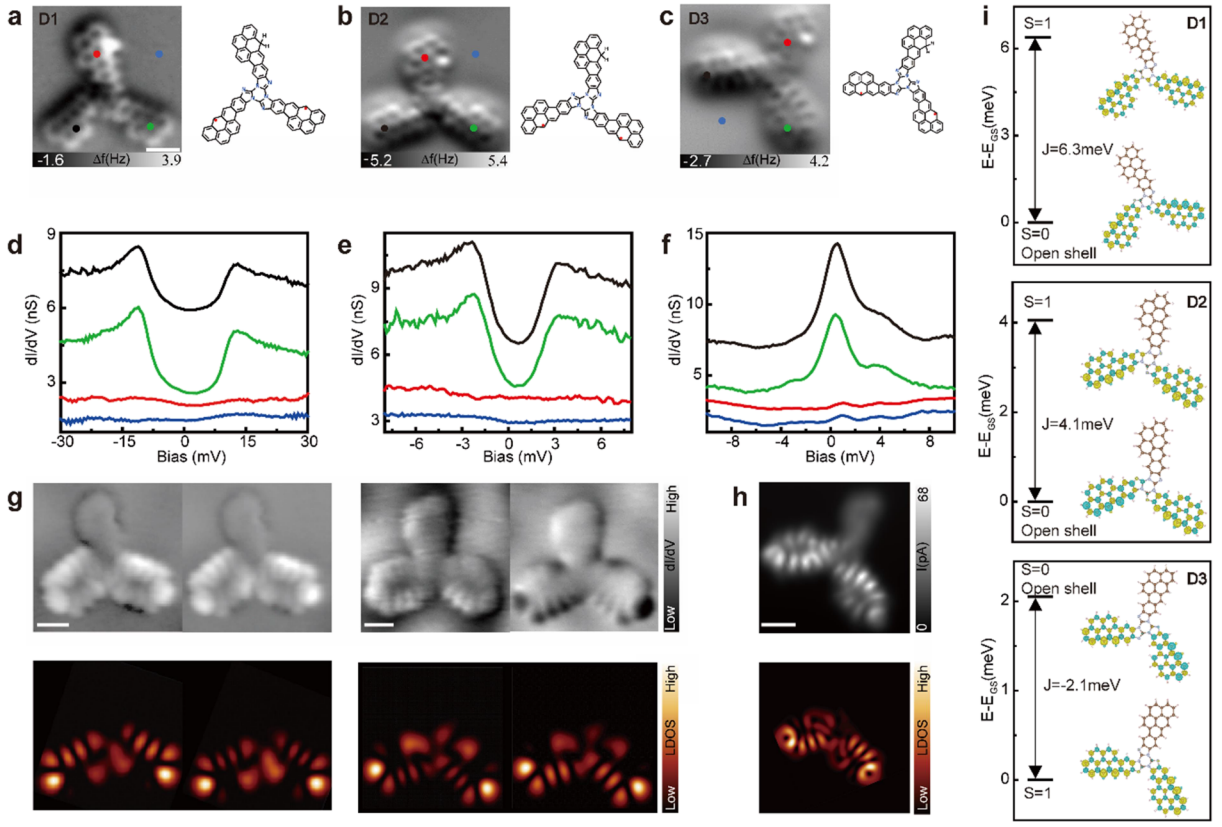

Figure 3. Electronic and magnetic characterization of representative diradical N-NGs. (a–c) nc-AFM images (resonant frequency: 26 kHz, oscillation amplitude: 80 pm) of D1, D2, and D3 and the corresponding chemical structures. (d–f) dI/dV spectra of D1, D2, and D3. The positions are marked by colored dots in Figure 2a–c. (g) Top: constant current dI/dV maps (set points from left to right: V = −15 mV, I = 40 pA; V = 15 mV, I = 40 pA; V = −100 mV, I = 80 pA; V = 100 mV, I = 80 pA) showing the spin excitation distribution of D1 and D2; bottom: the corresponding DFT-simulated LDOS images. (h) Constant height kondo map (bias: 2 mV) of D3 and the corresponding simulated LDOS image. (i) DFT-calculated energy levels of the ground state and the excited state of D1, D2, and D3. Inset: corresponding spin density distributions. Scale bars: 0.5 nm.

model reactant. In the C–H and N–H activation of imidazole, the calculated reaction barrier for the C–H activation (1.98 eV) is slightly 0.19 eV lower than that for the N–H activation (2.17 eV), suggesting that the C–H activation is a thermodynamically favorable step. In comparison, the reaction barrier of C–C coupling is 1.11 eV, which is 0.87 eV lower than that of the C–H activation. The reaction barriers of C–N coupling involving two reaction pathways are 1.48 and 1.05 eV, which is 0.5–0.93 eV lower than that of the C–H activation. These results demonstrate that the C–H and N–H activation is the rate-determining step of imidazole polymerization and two C–N coupling pathways are possible, resulting in the formation of diverse C–N coupling products. In addition, C–N coupling involves two possible pathways while C–C coupling only includes one pathway, supporting the experimental statistical results. Based on the experimental results and theoretical calculations, a tentative imidazole polymerization pathway on Au(111) can be proposed, as shown in Figure 2a and Figure S11a. The imidazoles first underwent C–H and N–H activation to form surface-bound carbon and nitrogen radicals, which underwent sequential C–C or C–N coupling to give diverse coupling product dimers. Finally, the C–N coupling of the dimer with other imidazole or imidazole-derived active radical intermediates may further undergo the intramolecular or intermolecular C–N coupling to afford the [2+2+2]-cyclotrimerization, [2+2+2+2]-cyclotetramerization, and other polymerization products, respectively.

Next, the trimerization products were pre-prepared in solution or solid-state from the imidazole derivative 2-phenoxy-1*H*-benzo[*d*]imidazole (the detailed synthetic procedure is given in the Supporting Information). Then the trimerization products (P1 and P2) were directly used as building blocks with the hope of obtaining N-NGs with homotactic configuration on Au(111). After deposition and thermal annealing to 290 °C, STM images (Figure 1e) show high abundance of clover-like structures (indicated by white dashed cycles) individually absorbed on the Au(111) surface, which can be assigned to the products N-NGs after cyclodehydrogenation. Further nc-AFM imaging shows that most N-NGs exhibit homotactic configuration in the N-doped core structure (the details are given in Figures S22–25), suggesting the high selectivity of imidazole [2+2+2]-cyclotrimerization in solution. Based on the experimentally observed results and previous literature report,[58] we proposed a tentative reaction pathway with the site-specific C–N coupling, where the reaction process mainly involves C–O activation to generate active phenolic radicals and N–H activation induced by phenolic radicals with the release of phenols (Figure 2b and Figure S11b). To get a better understanding of the difference between reactions in solution and on the surface, we performed Monte Carlo simulations with different flipping probabilities and coupling probabilities. As shown in Figures S12 and 13, MC simulations suggest that the coupling probability rather than the flip play a vital role in the reactions

https://doi.org/10.1021/jacs.2c10711
J. Am. Chem. Soc. 2023, 145, 7136–7146

toward highly selective homotactic trimers in-solution. Such results indicate that the on-surface and in-solution thermodynamics is similar. The reason behind the selective coupling of homotactic trimers in solution is due to their different reaction pathways as proposed in Figure 2.

Magnetic Exchange for Diradical N-NGs. We note that the π-radicals in nanographenes are quenched by hydrogen passivation, imaging as local bright protrusions in nc-AFM imaging due to the enhanced Pauli repulsion force of sp^3 carbons (Figure 1b,c). Such sp^3-passivated carbons can be controllably transferred into sp^2 carbons by applying a voltage pulse above 3 V to dissociate one hydrogen. Figure 3 shows three representative diradical nanographenes constructed by STM tip-induced atom manipulation, which are referred to as D1, D2, and D3 for convenience. For D1 (D2), the two unpaired spins are antiferromagnetically coupled as evidenced by spin-flip inelastic spectroscopy (Figure 3d,e), with a magnetic exchange coupling strength of 10.8 meV (1.7 meV). Spatially resolved dI/dV mappings show the local density of state (LDOS) distribution of nanographenes at a chosen bias. We note that the maps at 10 meV (2 meV) are the same as that at −10 mV (−2 meV) of D1 (D2) with dominant intensity at the bottom arms, which indicates that the step feature below and above the Fermi level should have the same origin. In the STM junction, the inelastic tunneling electrons excite the ground singlet state into the excited triplet state once the bias exceeds the exchange coupling J, which gives rise to a symmetric step feature at both the positive and negative biases. For D3, the two spins are ferromagnetically coupled as manifested as a sharp zero-bias Kondo resonance (Figure 3f).[59] As shown in Figure 3i, the Kondo mapping near zero bias reveals the spin density distribution of D3 with node patterns delocalized at the lower two arms.

Spin-unrestricted DFT calculations have been performed to determine exchange coupling J between the two spins in diradical nanographenes by comparing the total energies for different spin configurations. As shown in Figure 3i, we found that DFT calculations qualitatively agree with experiments. For D1 (D2), DFT calculations reveal that the spin-singlet state has lower total energy than that of the spin-triplet state, giving exchange coupling J = 6.3 meV (4.1 meV). The simulated STM images using singly occupied/unoccupied molecular orbitals in Figure 3h agree well with the experiments. For D3, the spin-triplet state is the ground state with exchange coupling J = −2.1 meV. In addition, the Heisenberg S = 1/2 model has been performed to elucidate the experimental observations. For ferromagnetically coupled S = 1/2 dimers, the ground state is the three-fold degenerated triplet state, and the first excited state is the spin-singlet state with an energy gap of J; for the antiferromagnetically coupled case, the ground state is the spin-singlet state, and the excited state is the degenerated triplet state. Using a perturbative approach to address the scattering process in the STM junction, the simulated dI/dV spectra fit with experiments very well using the exchange coupling of J = 10.8, 1.7, and −1.2 meV for D1, D2, and D3, respectively (Figure S14).[60] Our results indicate that DFT calculations using mean-field approximations qualitatively agree with Heisenberg spin model calculations for such two-spin systems, consistent with the previous studies.[5,11,13,61]

Exchange Mechanism of Diradical N-NGs and Comparison with Their Pure Hydrocarbon Counterparts. As shown in Figure 4a,b, the unpaired spin in each arm originates from sublattice imbalance, with dominated spin

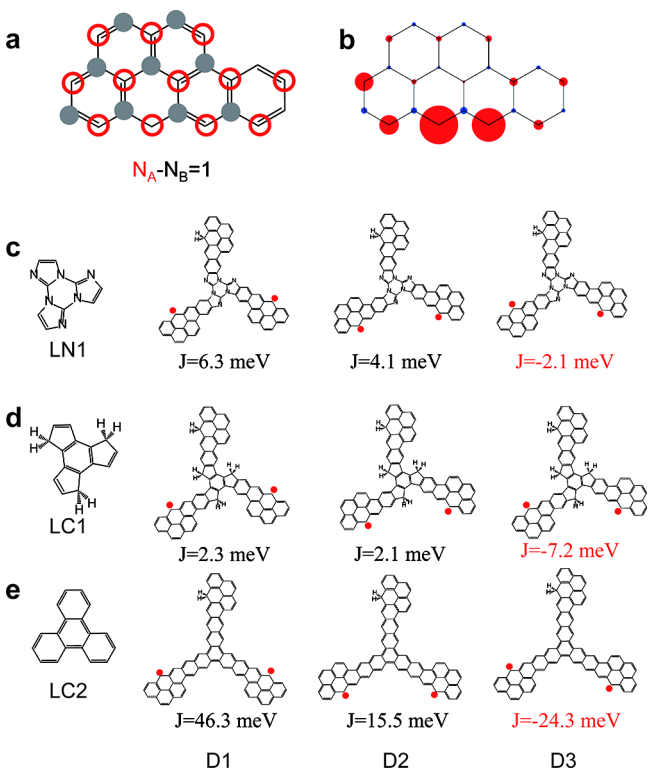

Figure 4. Comparison of N-NGs with pure hydrocarbon counterparts. (a) Sublattice imbalance of each arm with gray dots indicating sublattice A and open red circles indicating sublattice B. (b) Calculated spin density distribution of each arm. Red: spin-up density; blue: spin-down density. (c−e) Left: different linkers; right: chemical structures and the magnetic ground state of different dimer configurations.

density at sublattice A. There are three different diradical dimers when two arms are connected via a conjugated linker. For comparison, we calculated the magnetic ground states of three different linkers, as marked by LN1, LC1, and LC2 in Figure 4c−e. For all the linkers, the diradical dimer configurations D1 and D2 host antiferromagnetic exchange interaction with a singlet magnetic ground state; the diradical dimer configuration D3 hosts ferromagnetic exchange interaction with a triplet magnetic ground state. As illustrated in Figure S19, the π-electron topologies of LC1 linked nanographenes can be simplified as bipartite honeycomb graphs by removing the sp^3 carbon sites. The magnetic ground states can be determined by counting the number of carbon atoms in each sublattice of the graphene honeycomb lattice. For the D3 configuration, the sublattice imbalance is $N_A - N_B = 2$, which gives rise to a magnetic ground state of $S = (N_A - N_B)/2 = 1$ according to Lieb's theorem.[4] For the D1/D2 configuration, the sublattice imbalance is zero, which gives rise to either an open shell S = 0 singlet state or a closed-shell state. To determine the ground state, one can calculate the bipartite graph's nullity ($\eta = 2a - N$, where a is the maximum possible number of non-adjacent sites and N is the total number of sites).[2] The nullity is η = 2 for D1 and D2, which indicates that there are two zero eigen states of this graph, giving rise to an open-shell S = 0 singlet state due to topological frustration, similar to Clar's goblet structure.[5] In short, sublattice imbalance results in a ferromagnetic coupled state and topological frustration of π-electron topology gives rise to an antiferromagnetic coupled state for LC1 linked nanographenes.

https://doi.org/10.1021/jacs.2c10711
J. Am. Chem. Soc. 2023, 145, 7136−7146

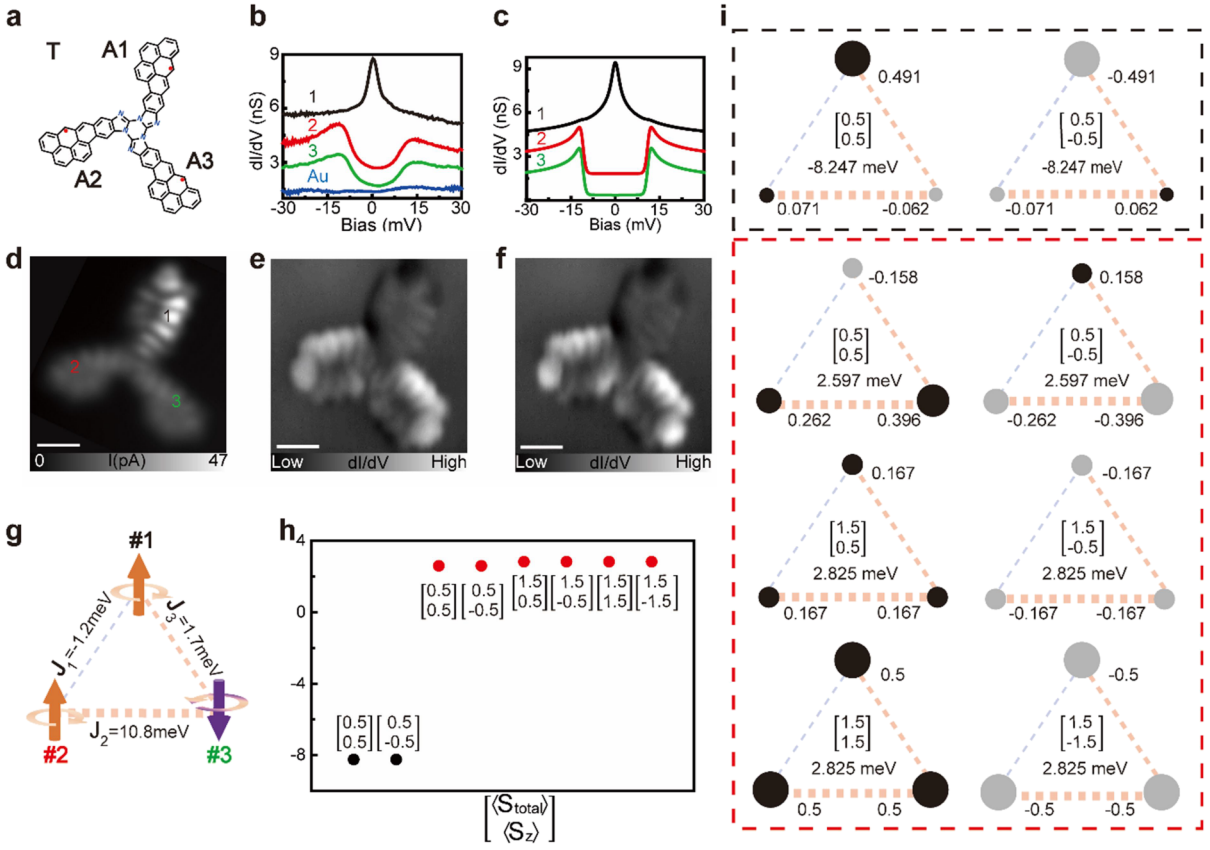

Figure 5. Collective quantum magnetism of a triradical N-NG with ground state $S = 1/2$. (a) Chemical structure of the triradical N-NG. (b) dI/dV spectra as taken at the positions marked in Figure 3d. (c) Simulated dI/dV spectra using a perturbative approach. (d) Constant-height current image (bias: 2 mV) of the triradical N-NG. (e, f) Constant-current dI/dV maps (set points from left to right: $V = -15$ mV, $I = 40$ pA; $V = 15$ mV, $I = 40$ pA). (g) Heisenberg spin model of the triradical N-NG. (h) Calculated spin states using the Heisenberg spin model. (i) Wave function of the ground states (black box) and excited states (red box) in Figure 3h. Scale bars: 0.5 nm.

For LC2 linked nanographenes, a similar exchange mechanism applies. As shown in Figure S20, the D3 configuration has sublattice imbalance $N_A - N_B = 2$ and thus has magnetic ground state $S = 1$; D1 and D2 configurations have a balanced sublattice and have a magnetic ground state of the $S = 0$ singlet state.

For LN1 linked nanographenes, the situation is more complicated since the pentagon rings break the bipartite sublattice symmetry of graphene. One cannot determine the magnetic ground by counting the sublattice imbalance or topological frustration nullity of π-electron topology. Here, we propose an empirical way to determine the magnetic ground state of LN1 linked nanographenes. As illustrated in Figure S21, we can determine the magnetic ground state through a local counting rule. Such an empirical method also applies for LC1, LC2, and LN1 nanographenes.

The magnetic exchange coupling strength between any two unpaired electrons in π-conjugated systems is a metric of the overlap of the two singly occupied orbitals, given by $J = 2U\sum_i |\varphi_1(i)|^2|\varphi_2(i)|^2$, where U denotes the Coulomb repulsion.[62] Qualitatively, the larger the overlap is, the stronger the exchange coupling strength. Since the singly occupied molecular orbital of each arm is asymmetric, the exchange coupling strength should be different for different dimer configurations. Additionally, we notice that LC2 linked nanographenes have the largest coupling strength, LN1 linked nanographenes the medium, and the LC1 linked nanographenes the smallest. This indicates that the conjugation degree of the linkers also plays an important role in the coupling strength.

Collective Quantum Magnetism in Triradical N-NG with Ground State $S = 1/2$. As shown in Figure 5a, we studied the spin states of a triradical N-NG with one radical per arm. We refer to the three arms as A1, A2, and A3. Differential tunneling spectroscopy measurements have been performed to resolve the low-lying spin states of the triradical N-NG. As shown in Figure 5b, a sharp zero-bias peak is observed only at A1, and a U gap is obtained at A2 and A3 with the same step energy at 10.8 meV. Spin-unrestricted DFT calculations reveal the presence of four spin states with equal intensity of spin density per arm: (1) the ground state is $S = 1/2$; (2) three excited spin states with the energy difference between the ground state and the three excited states of 4.7, 8.5, and 9.1 meV, respectively (cf. Figure S15). Apparently, DFT calculations fail to describe the experimental results, where the predicated three excitation gaps and the uniform spin density distributions clearly deviate from experiments. The discrepancies between experiments and DFT calculations are mainly from mean-field approximations, in which the wave functions are not the eigenstates of the total spin operator $\hat{S}^2$, but of the $\hat{S}_z$ projection. It is, therefore, inaccurate to describe spin states of open-shell nanographenes with more than two spins by using mean-field approximations. Many-body quantum chemistry methods should be more suitable but are limited to small systems due to their heavy computation load.

https://doi.org/10.1021/jacs.2c10711
J. Am. Chem. Soc. 2023, 145, 7136−7146

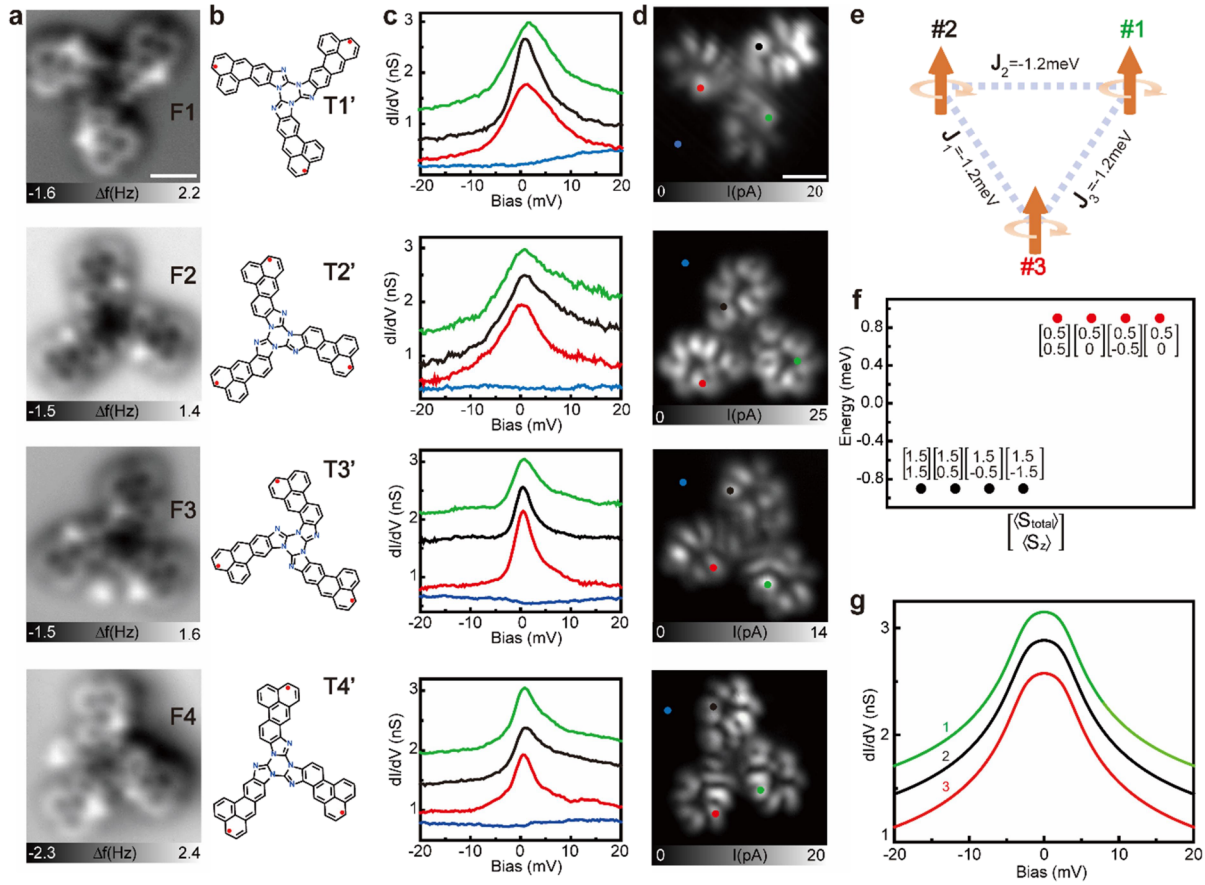

Figure 6. Collective quantum magnetism of triradical N-NGs with ground state S = 3/2. (a) nc-AFM images (resonant frequency: 26 kHz, oscillation amplitude: 80 pm) of four representative N-NGs. (b) Chemical structures of four representative triradical N-NGs as marked as T1′, T2′, T3′, and T4′. (c) dI/dV spectra of T1′, T2, T3′, and T4′ as taken at the positions as marked in Figure 4d. (d) Corresponding constant-height current images (bias: 2 mV). (e) Heisenberg spin model of triradical N-NGs. (f) Calculated spin states of triradical N-NGs using the Heisenberg spin model with parameters in (e). (g) Simulated dI/dV spectra based on the spin states in (f) using a perturbative approach. Scale bars: 0.5 nm.

The triradical N-NGs can be simplified as three spins with unequal exchange coupling with $J_1 = -1.2$, $J_2 = 1.7$, and $J_3 = 10.8$ meV (the exchange coupling values are obtained by fitting the experimental spectra of spin dimers as shown in Figure S14). The spin states of triradical N-NGs can be obtained by using the Heisenberg spin model with Hamiltonian $\hat{H} = \sum_{i \neq j} J_n \vec{S}_i \vec{S}_j$. In such a model, the exchange interaction among two spins is isotropic without considering magnetic anisotropy due to the negligible spin−orbit coupling of carbon/nitrogen materials. Such Heisenberg Hamiltonian can be strictly solved and give a complete set of ground spin states and excited states. For a system with three spins, there are in total eight eigen states. As shown in Figure 5h, the ground states have two-folder degeneracy, with quantum number $\hat{S}$ = 0.5, $\hat{S}_z = -0.5, 0.5$ (marked by black dots). The wave functions are shown in Figure 5i, where the ground states have dominant projected weight in the z direction at spin #1. This nicely agrees with experiments, where the ground states show dominant Kondo intensity at A1 (Figure 5d). There are six nearly degenerated excited states as marked by red dots. The wave functions of the two excited states with $\hat{S}$ = 0.5 have dominant weight at spin #2 and #3, while the wavefunctions of the four excited states with $\hat{S}$ = 1.5 have an equal weight per spin. In total, the six excited states have dominated weight at spin #2 and spin #3. The excited states also agree well with the experiment, where there is only one excitation gap (instead of three as predicted by DFT) with dominated spectra weight only at A2 and A3 (Figure 5e,f). For a better comparison, the dI/dV spectra are simulated using a perturbative approach based on the calculated Heisenberg spin states (Figure 5c), which finely reproduce all the experimental observations. The agreement between the Heisenberg spin model and experiments suggests that open-shell nanographenes with three spins host collective quantum magnetism.

Collective Quantum Magnetism in Triradical N-NGs with Ground State S = 3/2. Homotactic nanographenes can be fabricated by merging in-solution imidazole [2+2+2]-cyclotrimerization and on-surface cyclodehydrogenation. Due to the flip of the methylnaphthalene group after adsorption on Au(111), there are four different configurations of N-NGs with radicals that are quenched by hydrogens (Figure 6a). Using atom manipulation, we controllably dissociated sp^3 hydrogens to construct diradical nanographenes, which have ferromagnetic coupling for all the cases due to homotactic coupling of imidazole (Figures S22−25). Triradical nanographenes are further constructed, and their magnetic properties are resolved by dI/dV spectroscopy. As shown in Figure 6b, we refer to the four configurations with triradical N-NGs as T1′, T2′, T3′, and T4′. We find that all the homotactic trimers exhibit the same magnetic ground state. A sharp zero-bias Kondo peak is observed at each arm of all the T1′−T4′, suggesting the presence of a high spin state with S = 3/2. Kondo mapping

https://doi.org/10.1021/jacs.2c10711
J. Am. Chem. Soc. 2023, 145, 7136−7146

resolves the spatial distribution of spin density, which delocalizes inside the whole nanographenes (Figure 6d). These results suggest that magnetic coupling depends crucially on reaction coupling details. Homotactic coupling gives ferromagnetic coupling (Figure 3c and Figures S22−25), and heterotactic coupling results in antiferromagnetic coupling (Figure 3a,b).

The spin states of T1′−T4′ are elucidated using the Heisenberg spin model, with $J_1 = J_2 = J_3 = -1.2$ meV (Figure 6e). The calculated spin states are shown in Figure 6f. The ground states have four-fold degeneracy, with $\hat{S} = 1.5$, $\hat{S}_z = -1.5, -0.5, 0.5, 1.5$ (marked by black dots). The wave functions of the ground states have an equal weight per spin site, which agrees with the experimental observation of delocalized spin density distributions (Figure 6d). The excited states also have four-fold degeneracy, with $\hat{S} = 0.5$, $\hat{S}_z = -0.5, 0, 0.5, 0$ (marked by red dots). Based on Heisenberg spin states, we simulated the dI/dV spectra using a perturbative approach, which fit with experiments well (Figure 6g).

CONCLUSIONS

In summary, we fabricate a set of nitrogen-doped nanographenes with collective quantum magnetism via merging on-surface or in-solution imidazole [2+2+2]-cyclotrimerization and cyclodehydrogenation reactions. We reveal that imidazole [2+2+2]-cyclotrimerization occurs both on-surface and in-solution. On-surface imidazole trimerization gives rise to both homotactic and heterotactic trimers, while in-solution trimerization has high selectivity and results in pure homotactic trimers. Such differences can be attributed to the different ways of initiating reactions and coupling pathways. The magnetic spectroscopic features of these N-NGs are reproduced by Heisenberg spin model calculations. Our work demonstrates that heteroatom substitution provides a versatile toolbox for the efficient and selective fabrication of complex nanographenes which are difficult to realize by using precursors with pure carbons. The ability to engineer both the electronic properties and chemical reactivity by heteroatom substitution shows substantial potential to further realize designer quantum phases, such as quantum spin liquid states, in extended graphene frameworks.

ASSOCIATED CONTENT

Supporting Information

The Supporting Information is available free of charge at https://pubs.acs.org/doi/10.1021/jacs.2c10711.

Detailed descriptions of experimental and theoretical procedures, precursor synthesis, electronic structure of diradical homotactic nanographenes, and spectral simulation using a perturbative approach developed by M. Ternes (PDF)

AUTHOR INFORMATION

Corresponding Authors

Pei-Nian Liu − *Key Laboratory for Advanced Materials and Feringa Nobel Prize Scientist Joint Research Center, Frontiers Science Center for Materiobiology and Dynamic Chemistry, School of Chemistry and Molecular Engineering, East China University of Science & Technology, Shanghai 200237, China;* orcid.org/0000-0003-2014-2244; Email: liupn@ecust.edu.cn

Deng-Yuan Li − *Key Laboratory for Advanced Materials and Feringa Nobel Prize Scientist Joint Research Center, Frontiers Science Center for Materiobiology and Dynamic Chemistry, School of Chemistry and Molecular Engineering, East China University of Science & Technology, Shanghai 200237, China;* orcid.org/0000-0003-1721-9183; Email: dengyuanli@ecust.edu.cn

Shiyong Wang − *Key Laboratory of Artificial Structures and Quantum Control (Ministry of Education), Shenyang National Laboratory for Materials Science, School of Physics and Astronomy and Tsung-Dao Lee Institute, Shanghai Jiao Tong University, Shanghai 200240, China; Shanghai Research Center for Quantum Sciences, Shanghai 201315, China;* orcid.org/0000-0001-6603-9926; Email: shiyong.wang@sjtu.edu.cn

Authors

Gucheng Zhu − *Key Laboratory of Artificial Structures and Quantum Control (Ministry of Education), Shenyang National Laboratory for Materials Science, School of Physics and Astronomy, Shanghai Jiao Tong University, Shanghai 200240, China*

Yashi Jiang − *Key Laboratory of Artificial Structures and Quantum Control (Ministry of Education), Shenyang National Laboratory for Materials Science, School of Physics and Astronomy, Shanghai Jiao Tong University, Shanghai 200240, China*

Ying Wang − *Key Laboratory for Advanced Materials and Feringa Nobel Prize Scientist Joint Research Center, Frontiers Science Center for Materiobiology and Dynamic Chemistry, School of Chemistry and Molecular Engineering, East China University of Science & Technology, Shanghai 200237, China*

Bing-Xin Wang − *Key Laboratory for Advanced Materials and Feringa Nobel Prize Scientist Joint Research Center, Frontiers Science Center for Materiobiology and Dynamic Chemistry, School of Chemistry and Molecular Engineering, East China University of Science & Technology, Shanghai 200237, China*

Yuqiang Zheng − *Key Laboratory of Artificial Structures and Quantum Control (Ministry of Education), Shenyang National Laboratory for Materials Science, School of Physics and Astronomy, Shanghai Jiao Tong University, Shanghai 200240, China*

Yufeng Liu − *Key Laboratory of Artificial Structures and Quantum Control (Ministry of Education), Shenyang National Laboratory for Materials Science, School of Physics and Astronomy, Shanghai Jiao Tong University, Shanghai 200240, China*

Li-Xia Kang − *Key Laboratory for Advanced Materials and Feringa Nobel Prize Scientist Joint Research Center, Frontiers Science Center for Materiobiology and Dynamic Chemistry, School of Chemistry and Molecular Engineering, East China University of Science & Technology, Shanghai 200237, China*

Zhanbo Li − *College of New Materials and New Energies, Shenzhen Technology University, Shenzhen 518118, China*

Dandan Guan − *Key Laboratory of Artificial Structures and Quantum Control (Ministry of Education), Shenyang National Laboratory for Materials Science, School of Physics and Astronomy and Tsung-Dao Lee Institute, Shanghai Jiao Tong University, Shanghai 200240, China; Shanghai*

https://doi.org/10.1021/jacs.2c10711
J. Am. Chem. Soc. 2023, 145, 7136−7146

Research Center for Quantum Sciences, Shanghai 201315, China; orcid.org/0000-0002-3714-8813

Yaoyi Li − *Key Laboratory of Artificial Structures and Quantum Control (Ministry of Education), Shenyang National Laboratory for Materials Science, School of Physics and Astronomy and Tsung-Dao Lee Institute, Shanghai Jiao Tong University, Shanghai 200240, China; Shanghai Research Center for Quantum Sciences, Shanghai 201315, China*

Hao Zheng − *Key Laboratory of Artificial Structures and Quantum Control (Ministry of Education), Shenyang National Laboratory for Materials Science, School of Physics and Astronomy and Tsung-Dao Lee Institute, Shanghai Jiao Tong University, Shanghai 200240, China; Shanghai Research Center for Quantum Sciences, Shanghai 201315, China;* orcid.org/0000-0002-6495-874X

Canhua Liu − *Key Laboratory of Artificial Structures and Quantum Control (Ministry of Education), Shenyang National Laboratory for Materials Science, School of Physics and Astronomy and Tsung-Dao Lee Institute, Shanghai Jiao Tong University, Shanghai 200240, China; Shanghai Research Center for Quantum Sciences, Shanghai 201315, China;* orcid.org/0000-0003-2240-3559

Jinfeng Jia − *Key Laboratory of Artificial Structures and Quantum Control (Ministry of Education), Shenyang National Laboratory for Materials Science, School of Physics and Astronomy and Tsung-Dao Lee Institute, Shanghai Jiao Tong University, Shanghai 200240, China; Shanghai Research Center for Quantum Sciences, Shanghai 201315, China;* orcid.org/0000-0002-9900-281X

Tao Lin − *College of New Materials and New Energies, Shenzhen Technology University, Shenzhen 518118, China*

Complete contact information is available at: https://pubs.acs.org/10.1021/jacs.2c10711

Author Contributions

#G.Z., Y.J., and Y.W. contributed equally to this work.

Notes

The authors declare no competing financial interest.

■ ACKNOWLEDGMENTS

S.W. acknowledges the financial support from the National Key R&D Program of China (No. 2020YFA0309000), the National Natural Science Foundation of China (No. 11874258, No. 12074247), the Shanghai Municipal Science and Technology Qi Ming Xing Project (No. 20QA1405100), Fok Ying Tung Foundation for young researchers, YangYang Foundation, and SJTU (No. 21X010200846). D.-Y.L. acknowledges the financial support from the National Natural Science Foundation of China (No. 22272050) and the Shanghai Municipal Science and Technology Qi Ming Xing Project (No. 22QA1403000). This work was also supported by the Ministry of Science and Technology of China (Grant Nos. 2019YFA0308600, 2016YFA0301003, and 2016YFA0300403), NSFC (Grant Nos. 21925201, 22161160319, 11521404, 11634009, 92065201, 11874256, 11790313, and 11861161003), the Strategic Priority Research Program of Chinese Academy of Sciences (Grant No. XDB28000000), and the Science and Technology Commission of Shanghai Municipality (Grant Nos. 20ZR1414200, 2019SHZDZX01, 19JC1412701, and 20QA1405100).

■ REFERENCES

(1) Golor, M.; Wessel, S.; Schmidt, M. J. Quantum Nature of Edge Magnetism in Graphene. *Phys. Rev. Lett.* **2014**, *112*, No. 046601.
(2) Yazyev, O. V. Emergence of Magnetism in Graphene Materials and Nanostructures. *Rep. Prog. Phys.* **2010**, *73*, No. 056501.
(3) Clar, E. *Polycyclic Hydrocarbons*; Springer-Verlag: Berlin Heidelberg, 1964.
(4) Lieb, E. H. Two Theorems on the Hubbard Model. *Phys. Rev. Lett.* **1989**, *62*, 1201−1204.
(5) Mishra, S.; Beyer, D.; Eimre, K.; Kezilebieke, S.; Berger, R.; Gröning, O.; Pignedoli, C. A.; Müllen, K.; Liljeroth, P.; Ruffieux, P.; Feng, X.; Fasel, R. Topological Frustration Induces Unconventional Magnetism in a Nanographene. *Nat. Nanotechnol.* **2020**, *15*, 22−28.
(6) Li, C.; Liu, Y.; Liu, Y.; Xue, F.-H.; Guan, D.; Li, Y.; Zheng, H.; Liu, C.; Jia, J.; Liu, P.-N.; Li, D.-Y.; Wang, S. Topological Defects Induced High-Spin Quartet State in Truxene-Based Molecular Graphenoids. *CCS Chem.* **2023**, *5*, 695−703.
(7) Mishra, S.; Beyer, D.; Berger, R.; Liu, J.; Gröning, O.; Urgel, J. I.; Müllen, K.; Ruffieux, P.; Feng, X.; Fasel, R. Topological Defect-Induced Magnetism in a Nanographene. *J. Am. Chem. Soc.* **2020**, *142*, 1147−1152.
(8) Mishra, S.; Fatayer, S.; Fernández, S.; Kaiser, K.; Peña, D.; Gross, L. Nonbenzenoid High-Spin Polycyclic Hydrocarbons Generated by Atom Manipulation. *ACS Nano* **2022**, *16*, 3264−3271.
(9) Pavliček, N.; Mistry, A.; Majzik, Z.; Moll, N.; Meyer, G.; Fox, D. J.; Gross, L. Synthesis and Characterization of Triangulene. *Nat. Nanotechnol.* **2017**, *12*, 308−311.
(10) Song, S.; Su, J.; Telychko, M.; Li, J.; Li, G.; Li, Y.; Su, C.; Wu, J.; Lu, J. On-Surface Synthesis of Graphene Nanostructures with π-Magnetism. *Chem. Soc. Rev.* **2021**, *50*, 3238−3262.
(11) Zheng, Y.; Li, C.; Xu, C.; Beyer, D.; Yue, X.; Zhao, Y.; Wang, G.; Guan, D.; Li, Y.; Zheng, H.; Liu, C.; Liu, J.; Wang, X.; Luo, W.; Feng, X.; Wang, S.; Jia, J. Designer Spin Order in Diradical Nanographenes. *Nat. Commun.* **2020**, *11*, 6076.
(12) Su, X.; Li, C.; Du, Q.; Tao, K.; Wang, S.; Yu, P. Atomically Precise Synthesis and Characterization of Heptauthrene with Triplet Ground State. *Nano Lett.* **2020**, *20*, 6859−6864.
(13) Zheng, Y.; Li, C.; Zhao, Y.; Beyer, D.; Wang, G.; Xu, C.; Yue, X.; Chen, Y.; Guan, D.-D.; Li, Y.-Y.; Zheng, H.; Liu, C.; Luo, W.; Feng, X.; Wang, S.; Jia, J. Engineering of Magnetic Coupling in Nanographene. *Phys. Rev. Lett.* **2020**, *124*, No. 147206.
(14) Li, J.; Sanz, S.; Corso, M.; Choi, D. J.; Peña, D.; Frederiksen, T.; Pascual, J. I. Single Spin Localization and Manipulation in Graphene Open-Shell Nanostructures. *Nat. Commun.* **2019**, *10*, 200.
(15) Li, J.; Sanz, S.; Castro-Esteban, J.; Vilas-Varela, M.; Friedrich, N.; Frederiksen, T.; Peña, D.; Pascual, J. I. Uncovering the Triplet Ground State of Triangular Graphene Nanoflakes Engineered with Atomic Precision on a Metal Surface. *Phys. Rev. Lett.* **2020**, *124*, No. 177201.
(16) de Oteyza, D. G.; Frederiksen, T. Carbon-Based Nanostructures as a Versatile Platform for Tunable π-Magnetism. *J. Phys.: Condens. Matter* **2022**, *34*, 443001.
(17) Sun, Z.; Wu, J. Open-Shell Polycyclic Aromatic Hydrocarbons. *J. Mater. Chem.* **2012**, *22*, 4151−4160.
(18) Grill, L.; Hecht, S. Covalent On-Surface Polymerization. *Nat. Chem.* **2020**, *12*, 115−130.
(19) Grill, L.; Dyer, M.; Lafferentz, L.; Persson, M.; Peters, M. V.; Hecht, S. Nano-Architectures by Covalent Assembly of Molecular Building Blocks. *Nat. Nanotechnol.* **2007**, *2*, 687−691.
(20) Cheng, S.; Xue, Z.; Li, C.; Liu, Y.; Xiang, L.; Ke, Y.; Yan, K.; Wang, S.; Yu, P. On-Surface Synthesis of Triangulene Trimers via Dehydration Reaction. *Nat. Commun.* **2022**, *13*, 1705.
(21) Hieulle, J.; Castro, S.; Friedrich, N.; Vegliante, A.; Lara, F. R.; Sanz, S.; Rey, D.; Corso, M.; Frederiksen, T.; Pascual, J. I.; Peña, D. On-Surface Synthesis and Collective Spin Excitations of a Triangulene-Based Nanostar. *Angew. Chem., Int. Ed.* **2021**, *60*, 25224−25229.
(22) Mishra, S.; Beyer, D.; Eimre, K.; Liu, J.; Berger, R.; Gröning, O.; Pignedoli, C. A.; Müllen, K.; Fasel, R.; Feng, X.; Ruffieux, P.

Synthesis and Characterization of π-Extended Triangulene. *J. Am. Chem. Soc.* **2019**, *141*, 10621−10625.
(23) Mishra, S.; Beyer, D.; Eimre, K.; Ortiz, R.; Fernández-Rossier, J.; Ber, R. Collective All-Carbon Magnetism in Triangulene Dimers. *Angew. Chem., Int. Ed.* **2020**, *59*, 12041−12047.
(24) Su, J.; Telychko, M.; Hu, P.; Macam, G.; Mutombo, P.; Zhang, H.; Bao, Y.; Cheng, F.; Huang, Z.-Q.; Qiu, Z.; Tan, S. J. R.; Lin, H.; Jelínek, P.; Chuang, F.-C.; Wu, J.; Lu, J. Atomically Precise Bottom-up Synthesis of π-Extended [5]Triangulene. *Sci. Adv.* **2019**, *5*, No. eaav7717.
(25) Wang, T.; Berdonces-Layunta, A.; Friedrich, N.; Vilas-Varela, M.; Calupitan, J. P.; Pascual, J. I.; Peña, D.; Casanova, D.; Corso, M.; de Oteyza, D. G. Aza-Triangulene: On-Surface Synthesis and Electronic and Magnetic Properties. *J. Am. Chem. Soc.* **2022**, *144*, 4522−4529.
(26) Zhao, Y.; Jiang, K.; Li, C.; Liu, Y.; Xu, C.; Zheng, W.; Guan, D.; Li, Y.; Zheng, H.; Liu, C.; Luo, W.; Jia, J.; Zhuang, X.; Wang, S. Precise Control of π-Electron Magnetism in Metal-Free Porphyrins. *J. Am. Chem. Soc.* **2020**, *142*, 18532−18540.
(27) Zhao, Y.; Jiang, K.; Li, C.; Liu, Y.; Zhu, G.; Pizzochero, M.; Kaxiras, E.; Guan, D.; Li, Y.; Zheng, H.; Liu, C.; Jia, J.; Qin, M.; Zhuang, X.; Wang, S. Quantum Nanomagnets in On-Surface Metal-Free Porphyrin Chains. *Nat. Chem.* **2023**, *15*, 53−60.
(28) Mateo, L. M.; Sun, Q.; Liu, S.-X.; Bergkamp, J. J.; Eimre, K.; Pignedoli, C. A.; Ruffieux, P.; Decurtins, S.; Bottari, G.; Fasel, R.; Torres, T. On-Surface Synthesis and Characterization of Triply Fused Porphyrin-Graphene Nanoribbon Hybrids. *Angew. Chem., Int. Ed.* **2020**, *59*, 1334−1339.
(29) Mishra, S.; Catarina, G.; Wu, F.; Ortiz, R.; Jacob, D.; Eimre, K.; Ma, J.; Pignedoli, C. A.; Feng, X.; Ruffieux, P.; Fernández-Rossier, J.; Fasel, R. Observation of Fractional Edge Excitations in Nanographene Spin Chains. *Nature* **2021**, *598*, 287−292.
(30) Liu, Y.; Li, C.; Xue, F.-H.; Wang, Y.; Huang, H.; Yang, H.; Chen, J.; Guan, D.; Li, Y.; Zheng, H.; Liu, C.; Qin, M.; Wang, X.; Li, D.-Y.; Liu, P.-N.; Wang, S.; Jia, J. Quantum Phase Transition in Magnetic Nanographenes on a Lead Superconductor. *arXiv* **2022**, DOI: 10.48550/arXiv.2207.05313.
(31) Cai, J.; Pignedoli, C. A.; Talirz, L.; Ruffieux, P.; Söde, H.; Liang, L.; Meunier, V.; Berger, R.; Li, R.; Feng, X.; Müllen, K.; Fasel, R. Graphene Nanoribbon Heterojunctions. *Nat. Nanotechnol.* **2014**, *9*, 896−900.
(32) Nguyen, G. D.; Tsai, H.-Z.; Omrani, A. A.; Marangoni, T.; Wu, M.; Rizzo, D. J.; Rodgers, G. F.; Cloke, R. R.; Durr, R. A.; Sakai, Y.; Liou, F.; Aikawa, A. S.; Chelikowsky, J. R.; Louie, S. G.; Fischer, F. R.; Crommie, M. F. Atomically Precise Graphene Nanoribbon Heterojunctions from a Single Molecular Precursor. *Nat. Nanotechnol.* **2017**, *12*, 1077−1082.
(33) Blackwell, R. E.; Zhao, F.; Brooks, E.; Zhu, J.; Piskun, I.; Wang, S.; Delgado, A.; Lee, Y.-L.; Louie, S. G.; Fischer, F. R. Spin Splitting of Dopant Edge State in Magnetic Zigzag Graphene Nanoribbons. *Nature* **2021**, *600*, 647−652.
(34) Friedrich, N.; Brandimarte, P.; Li, J.; Saito, S.; Yamaguchi, S.; Pozo, I.; Peña, D.; Frederiksen, T.; Garcia-Lekue, A.; Sánchez-Portal, D.; Pascual, J. I. Magnetism of Topological Boundary States Induced by Boron Substitution in Graphene Nanoribbons. *Phys. Rev. Lett.* **2020**, *125*, No. 146801.
(35) Kawai, S.; Saito, S.; Osumi, S.; Yamaguchi, S.; Foster, A. S.; Spijker, P.; Meyer, E. Atomically Controlled Substitutional Boron-Doping of Graphene Nanoribbons. *Nat. Commun.* **2015**, *6*, 8098.
(36) Zhang, Y.; Lu, J.; Li, Y.; Li, B.; Ruan, Z.; Zhang, H.; Hao, Z.; Sun, S.; Xiong, W.; Gao, L.; Chen, L.; Cai, J. On-Surface Synthesis of a Nitrogen-Doped Graphene Nanoribbon with Multiple Substitutional Sites. *Angew. Chem., Int. Ed.* **2022**, *61*, No. e202204736.
(37) Kawai, S.; Nakatsuka, S.; Hatakeyama, T.; Pawlak, R.; Meier, T.; Tracey, J.; Meyer, E.; Foster, A. S. Multiple Heteroatom Substitution to Graphene Nanoribbon. *Sci. Adv.* **2018**, *4*, No. eaar7181.
(38) Wen, E. C. H.; Jacobse, P. H.; Jiang, J.; Wang, Z.; McCurdy, R. D.; Louie, S. G.; Crommie, M. F.; Fischer, F. R. Magnetic Interactions in Substitutional Core-Doped Graphene Nanoribbons. *J. Am. Chem. Soc.* **2022**, *144*, 13696−13703.
(39) Biswas, K.; Urgel, J. I.; Xu, K.; Ma, J.; Sánchez-Grande, A.; Mutombo, P.; Gallardo, A.; Lauwaet, K.; Mallada, B.; de la Torre, B.; Matěj, A.; Gallego, J. M.; Miranda, R.; Jelínek, P.; Feng, X.; Écija, D. On-Surface Synthesis of a Dicationic Diazahexabenzocoronene Derivative on the Au(111) Surface. *Angew. Chem., Int. Ed.* **2021**, *60*, 25551−25556.
(40) Piskun, I.; Blackwell, R.; Jornet-Somoza, J.; Zhao, F.; Rubio, A.; Louie, S. G.; Fischer, F. R. Covalent C−N Bond Formation through a Surface Catalyzed Thermal Cyclodehydrogenation. *J. Am. Chem. Soc.* **2020**, *142*, 3696−3700.
(41) Eimre, K.; Urgel, J. I.; Hayashi, H.; Di Giovannantonio, M.; Ruffieux, P.; Sato, S.; Otomo, S.; Chan, Y. S.; Aratani, N.; Passerone, D.; Gröning, O.; Yamada, H.; Fasel, R.; Pignedoli, C. A. On-Surface Synthesis and Characterization of Nitrogen-Substituted Undecacenes. *Nat. Commun.* **2022**, *13*, 511−511.
(42) Kocić, N.; Liu, X.; Chen, S.; Decurtins, S.; Krejčí, O.; Jelínek, P.; Repp, J.; Liu, S.-X. Control of Reactivity and Regioselectivity for On-Surface Dehydrogenative Aryl−Aryl Bond Formation. *J. Am. Chem. Soc.* **2016**, *138*, 5585−5593.
(43) Li, D.-Y.; Wang, Y.; Hou, X.-Y.; Ren, Y.-T.; Kang, L.-X.; Xue, F.-H.; Zhu, Y.-C.; Liu, J.-W.; Liu, M.; Shi, X.-Q.; Qiu, X.; Liu, P.-N. On-Surface Synthesis of [3]Radialenes via [1+1+1] Cycloaddition. *Angew. Chem., Int. Ed.* **2022**, *61*, No. e202117714.
(44) Riss, A.; Richter, M.; Paz, A. P.; Wang, X.-Y.; Raju, R.; He, Y.; Ducke, J.; Corral, E.; Wuttke, M.; Seufert, K.; Garnica, M.; Rubio, A.; Barth, J.; Narita, A.; Müllen, K.; Berger, R.; Feng, X.; Palma, C.-A.; Auwärter, W. Polycyclic Aromatic Chains on Metals and Insulating Layers by Repetitive [3+2] Cycloadditions. *Nat. Commun.* **2020**, *11*, 1490.
(45) Díaz Arado, O.; Mönig, H.; Wagner, H.; Franke, J.-H.; Langewisch, G.; Held, P. A.; Studer, A.; Fuchs, H. On-Surface Azide−Alkyne Cycloaddition on Au(111). *ACS Nano* **2013**, *7*, 8509−8515.
(46) Yang, B.; Niu, K.; Haag, F.; Cao, N.; Zhang, J.; Zhang, H.; Li, Q.; Allegretti, F.; Björk, J.; Barth, J. V.; Chi, L. Abiotic Formation of an Amide Bond via Surface-Supported Direct Carboxyl−Amine Coupling. *Angew. Chem., Int. Ed.* **2022**, *61*, No. e202113590.
(47) Fan, Q.; Luy, J.-N.; Liebold, M.; Greulich, K.; Zugermeier, M.; Sundermeyer, J.; Tonner, R.; Gottfried, J. M. Template-Controlled on-Surface Synthesis of a Lanthanide Supernaphthalocyanine and Its Open-Chain Polycyanine Counterpart. *Nat. Commun.* **2019**, *10*, 5049.
(48) Li, D.-Y.; Li, S.-W.; Xie, Y.-L.; Hua, X.; Long, Y.-T.; Wang, A.; Liu, P.-N. On-Surface Synthesis of Planar Dendrimers via Divergent Cross-Coupling Reaction. *Nat. Commun.* **2019**, *10*, 2414.
(49) Biagiotti, G.; Perini, I.; Richichi, B.; Cicchi, S. Novel Synthetic Approach to Heteroatom Doped Polycyclic Aromatic Hydrocarbons: Optimizing the Bottom-Up Approach to Atomically Precise Doped Nanographenes. *Molecules* **2021**, *26*, 6306.
(50) Fu, Y.; Yang, H.; Gao, Y.; Huang, L.; Berger, R.; Liu, J.; Lu, H.; Cheng, Z.; Du, S.; Gao, H.-J.; Feng, X. On-Surface Synthesis of NBN-Doped Zigzag-Edged Graphene Nanoribbons. *Angew. Chem., Int. Ed.* **2020**, *59*, 8873−8879.
(51) Pawlak, R.; Liu, X.; Ninova, S.; D'Astolfo, P.; Drechsel, C.; Sangtarash, S.; Häner, R.; Decurtins, S.; Sadeghi, H.; Lambert, C. J.; Aschauer, U.; Liu, S.-X.; Meyer, E. Bottom-up Synthesis of Nitrogen-Doped Porous Graphene Nanoribbons. *J. Am. Chem. Soc.* **2020**, *142*, 12568−12573.
(52) Vo, T. H.; Perera, U. G. E.; Shekhirev, M.; Mehdi Pour, M.; Kunkel, D. A.; Lu, H.; Gruverman, A.; Sutter, E.; Cotlet, M.; Nykypanchuk, D.; Zahl, P.; Enders, A.; Sinitskii, A.; Sutter, P. Nitrogen-Doping Induced Self-Assembly of Graphene Nanoribbon-Based Two-Dimensional and Three-Dimensional Metamaterials. *Nano Lett.* **2015**, *15*, 5770−5777.
(53) Feng, Z.; Mazaheripour, A.; Dibble, D. J.; Wagner, P.; Czap, G.; Kladnik, G.; Cossaro, A.; Verdini, A.; Floreano, L.; Bavdek, G.; Ho, W.; Comelli, G.; Cvetko, D.; Morgante, A.; Gorodetsky, A. A. Bottom-up Synthesis of Nitrogen-Containing Graphene Nanoribbons

from the Tetrabenzopentacene Molecular Motif. *Carbon* **2020**, *170*, 677−684.
(54) Skidin, D.; Eisenhut, F.; Richter, M.; Nikipar, S.; Krüger, J.; Ryndyk, D. A.; Berger, R.; Cuniberti, G.; Feng, X.; Moresco, F. On-Surface Synthesis of Nitrogen-Doped Nanographenes with 5−7 Membered Rings. *Chem. Commun.* **2019**, *55*, 4731−4734.
(55) Pawlak, R.; Liu, X.; Ninova, S.; D'Astolfo, P.; Drechsel, C.; Liu, J.-C.; Häner, R.; Decurtins, S.; Aschauer, U.; Liu, S.-X.; Meyer, E. On-Surface Synthesis of Nitrogen-Doped Kagome Graphene. *Angew. Chem., Int. Ed.* **2021**, *60*, 8370−8375.
(56) Biswas, K.; Urbani, M.; Sánchez-Grande, A.; Soler-Polo, D.; Lauwaet, K.; Matěj, A.; Mutombo, P.; Veis, L.; Brabec, J.; Pernal, K.; Gallego, J. M.; Miranda, R.; Écija, D.; Jelínek, P.; Torres, T.; Urgel, J. I. Interplay between π-Conjugation and Exchange Magnetism in One-Dimensional Porphyrinoid Polymers. *J. Am. Chem. Soc.* **2022**, *144*, 12725−12731.
(57) Bhattacharya, R.; Ray, S.; Ray, J.; Ghosh, A. Thermally Induced Oxidative Trimerization of Benzimidazole by Copper(II) Chloride in the Solid State. *Open Chem.* **2003**, *1*, 427−440.
(58) Ishida, S.; Fukushima, Y.; Sekiguchi, S.; Matsui, K. Tris-(Benzimidazo)-1,3,5-Triazine from the Thermolysis of 2-Aryloxybenzimidazoles. *Bull. Chem. Soc. Jpn.* **1975**, *48*, 956−959.
(59) Kondo, J. Resistance Minimum in Dilute Magnetic Alloys. *Prog. Theor. Phys.* **1964**, *32*, 37−49.
(60) Ternes, M. Spin Excitations and Correlations in Scanning Tunneling Spectroscopy. *New J. Phys.* **2015**, *17*, No. 063016.
(61) Wang, T.; Sanz, S.; Castro-Esteban, J.; Lawrence, J.; Berdonces-Layunta, A.; Mohammed, M. S. G.; Vilas-Varela, M.; Corso, M.; Peña, D.; Frederiksen, T.; de Oteyza, D. G. Magnetic Interactions Between Radical Pairs in Chiral Graphene Nanoribbons. *Nano Lett.* **2022**, *22*, 164−171.
(62) Ortiz, R.; Boto, R. A.; García-Martínez, N.; Sancho-García, J. C.; Melle-Franco, M.; Fernández-Rossier, J. Exchange Rules for Diradical π-Conjugated Hydrocarbons. *Nano Lett.* **2019**, *19*, 5991−5997.

https://doi.org/10.1021/jacs.2c10711
J. Am. Chem. Soc. 2023, 145, 7136−7146